Discrimination of Methanol and Ethanol Vapors by the Use of a Single Optical Sensor with a Microporous Sensitive Layer

ARTICLE *in* ANALYTICAL CHEMISTRY · OCTOBER 2002

Impact Factor: 5.64 · DOI: 10.1021/ac0258204 · Source: PubMed

3 AUTHORS, INCLUDING:

Frank Dieterle
Novartis
45 PUBLICATIONS **1,905** CITATIONS
SEE PROFILE

Günter Gauglitz
University of Tuebingen
350 PUBLICATIONS **9,011** CITATIONS
SEE PROFILE

Anal. Chem. **2002,** *74,* 4781−4787

Discrimination of Methanol and Ethanol Vapors by the Use of a Single Optical Sensor with a Microporous Sensitive Layer

Birgit Kieser,* Frank Dieterle, and Günter Gauglitz

Institute of Physical and Theoretical Chemistry, University of Tübingen, Auf der Morgenstelle 8, 72076 Tübingen, Germany

The sorption of methanol and ethanol vapors by a microporous glassy polycarbonate is studied. The increase of the refractive index of the polymer during analyte sorption is measured by surface plasmon resonance. Both analytes are sorbed into the micropores of the polymer showing different diffusion kinetics. The sensor response during analyte exposure is subdivided into different time channels. By evaluating this additional data dimension by neural networks, a simultaneous multicomponent analysis of binary mixtures of ethanol and methanol vapors is possible using the sensor response of only one single sensor. A feature extraction results in an interpretable model and an improved prediction with errors of 2.0% for methanol and 2.4% for ethanol.

There have been numerous reports on the detection of volatile organic compounds by polymer-based sensors such as bulk or surface acoustic wave sensors, various integrated optical sensors, and devices based on the reflectometric interference spectroscopy and surface plasmon resonance (SPR). A wide variety of polymers are used as sensitive layers, which are usually selective to whole classes of analytes. A multicomponent analysis of mixtures consisting of various analytes is possible by an array of sensors showing different selectivity and sensitivity for these analytes. By evaluating the sensor responses with model-based multivariate methods or neural networks, a classification and quantification of analytes in mixtures is possible.[1−7]

Recently, the exploitation of temporal information of sensor responses has been reported by several groups. In these reports, this additional information allowed the qualitative and quantitative detection of several analytes by a reduced number of sensors: Yan et al.[8] quantified a binary mixture of solvents in water by a single reflectometric interference spectroscopic sensor since the time shift of the highest signal after analyte exposure depended on the composition of the mixture. The components of binary and ternary mixtures of organic analytes in water could also be determined by one single amperometric sensor.[9,10] Thereby, the consumption of oxygen by the metabolism of microorganisms with different time constants for the analytes was detected. In the gaseous phase, the time-resolved measurement was used in combination with sensor arrays to get additional independent variables. By time-resolved measurements with an array of quartz microbalances coated with three different polymer films, the classification of six solvent vapors could be improved compared to the classification using only the saturation mass.[11] Johnson et al.[12] classified 20 different analytes with only 4 fiber-optic sensors and also classified these analytes semiquantitatively into low, medium, and high analyte concentrations using 10 fiber-optic sensors with 90% of the test data being assigned to the correct concentration class.

Podgorsek et al.[13] used a glassy polyimide for the detection of methanol and ethanol and showed the difference of the response times, which could be used for the discrimination of both analytes. However, a detection of both analytes in mixtures was not performed. The work presented here focuses on a simultaneous quantification of methanol and ethanol in binary mixtures using time-resolved measurements with a single SPR sensor setup based on a microporous polycarbonate. The evanescent field method SPR has been chosen as the single sensor setup for the time-resolved measurements since the main influence of the signal is given near the transducer surface. The signal does not rise as fast as the signal of bulk sensors; however, the maximum of the signal appears at the same time. First, the sorption process of the single analytes is investigated in respect to changes of the refractive index over analyte exposure time, in respect to changes of the refractive index caused by different concentrations and in respect to the long-term stability of the polymer. Then, two data sets of binary mixtures of methanol and ethanol are measured,

* To whom correspondence should be addressed. Phone: +49(0)7071/2978760. Fax: +49(0)7071/295960. E-mail: birgit.kieser@ipc.uni-tuebingen.de.

(1) Jurs, P. C.; Bakken, G. A.; McClelland, H. E. *Chem. Rev.* **2000**, *100*, 2649−2678.
(2) Dolemann, B. J.; Lonergan, M. C.; Severin, E. J.; Vaid, T. P.; Lewis, N. S. *Anal. Chem.* **1998**, *70*, 4177−4190.
(3) Park, J.; Groves, W. A.; Zellers, E. T. *Anal. Chem.* **1999**, *71*, 3877−3886.
(4) Seemann, J.; Rapp, F.-R.; Zell, A.; Gauglitz, G. *Fresenius J. Anal. Chem.* **1997**, *359*, 100−106.
(5) Shaffer, R. E.; Rose-Pehrsson, S. L.; McGill, R. A. *Anal. Chim. Acta* **1999**, *384*, 305−317.
(6) Hierlemann, A.; Weimar, U.; Kraus, G.; Gauglitz, G.; Göpel, W. *Sens. Mater.* **1995**, *7*, 179−189.
(7) Grate, Y. W.; Wise, B. M. *Anal. Chem.* **2001**, *73*, 2239−2244.
(8) Yan, H. M.; Kraus, G.; Gauglitz, G. *Anal. Chim. Acta* **1995**, *312*, 1−8.
(9) Slama, M.; Zaborosch, C.; Wienke, D.; Spener, F. *Anal. Chem.* **1996**, *68*, 3845−3850.
(10) Plegge, V.; Slama, M.; Süselbeck, B.; Wienke, D.; Spener, F.; Knoll, M.; Zaborosch, C. *Anal. Chem.* **2000**, *72*, 2937−2942.
(11) Sugimoto, I.; Nakamura, M.; Kuwano, H. *Sens. Actuators, B* **1993**, *10*, 117−122.
(12) Johnson, S. R.; Sutter, J. M.; Engelhardt, H. L.; Jurs, P. C.; White, J.; Kauer, J. S.; Dickinson, T. A.; Walt, D. R. *Anal. Chem.* **1997**, *69*, 4641−4648.
(13) Podgorsek, R. P.; Franke, H.; Woods, J.; Morrill, S. *Sens. Actuators, B* **1998**, *51*, 146−151.

10.1021/ac0258204 CCC: $22.00
Published on Web 08/22/2002

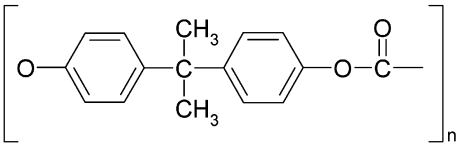

Figure 1. Structure of the polycarbonate Makrolon M2400.

whereby the changes of the refractive index are recorded over time and are divided into different time channels. As the relationship between the sensor responses of the different time channels and the concentrations of the analytes is nonlinear, the data are evaluated by use of neural networks. Finally, a feature selection of the most important time channels is performed, resulting in an improved prediction of the test data and in a smaller and better interpretable model.

EXPERIMENTAL SECTION

Surface Plasmon Resonance. A white light SPR setup was used, which is sensitive to changes of the refractive index of the sensitive layer. Surface plasmons are excited on a silver layer, and the sensitive layer is probed by the evanescent field of the surface plasmons, which reaches into the sensitive layer and thereby decays exponentially. The probe depth δ^{I}_{zv}, which is the distance from the interface between the metal and the sensitive layer to the depth of the sensitive layer where the intensity has decreased to 1/eth, is given by Johansen et al.[14] and Jung et al.:[15]

$$\delta^{I}_{zv} = \left|\frac{i\lambda\sqrt{\epsilon_{2,re} + n_3^2}}{4\pi n_3^2}\right| \qquad (1)$$

The SPR setup is based on the Kretschmann configuration.[16] The parallel-polarized polychromatic light (5-V/5-W krypton with integrated reflector, Welch Allyn, New York) is focused on the prism at a fixed angle (63°). Surface plasmons are excited at the prism's back surface. The modulated output light is coupled into a multimode fiber and detected with a diode array spectrometer (MMS Zeiss, Jena, Germany). As the surface plasmon wave is only excited by the TM mode, the TE mode is used as a reference signal. Temperature control was achieved with a thermoregulator (F34-MD Julabo, Seelbach, Germany).

Coating Materials and Procedures. The substrate consisted of silver evaporated onto a glass prism (half-cylindric, ground 20 × 40 mm, $n_D = 1.92286$ NPH2, Ohara Corp.) by using a vacuum evaporation system (Pfeiffer Vacuum GmbH, Wetzlar, Germany). The silver was deposited under high-vacuum conditions (10^{-6}–10^{-7} mbar) at a rate of about 0.6–1 nm s^{-1}. The metal thickness was monitored by a crystal oscillator. Approximately 50 nm of silver was deposited onto the glass. A 40-μL aliquot of a polycarbonate solution (Makrolon, M2400 (Figure 1), Bayer AG, Leverkusen, Germany, 1.7 wt %) in chloroform was spin-coated (Convac 2001, Wiernsheim, Germany) for 40 s with 3000 rpm on the silver layer of the NPH2 glass prism mentioned before. The prepared polymer layer had a thickness of ~300 nm, which was determined by a surface profilometer (Alpha Step 500, Tencor Instruments). According to eq 1, the probe depth is 98 nm. Thus, the sensitive layer has more than 3 times the probe depth.

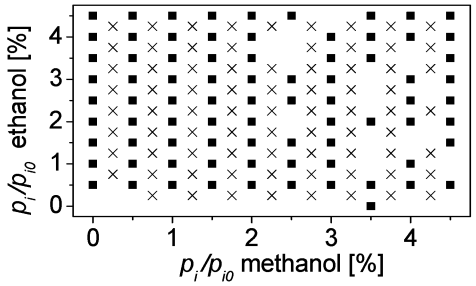

Figure 2. Experimental design of the calibration data set and the test data set. Calibration data are represented by squares, and test data are represented by crosses.

The dielectric constants of silver were determined by spectral ellipsometry (ES4G, Sopra). The Cauchy parameters of the prism are $A = 1.855\,31$, $B = 2.3 \times 10^4$ nm^2, and $C = 1.3 \times 10^8$ nm^4. Using these parameters, the change of the refractive index of the sensitive layer was determined from the change of the resonance wavelength by the Fresnel equations.

Data Sets. In addition to several single-analyte measurements, two data sets were recorded for a multicomponent analysis of binary mixtures. The first data set is a nine-level full factorial design whereby the relative saturation pressures (p_i/p_{i0}) of methanol and ethanol have been varied between 0 and 0.045. The partial pressure p_i was referenced to the saturation pressure p_{i0} at the measuring temperature of 30 °C. This data set was used for training of the neural networks and for feature selection and thus will be further referred to as the calibration set. The second data set is an eight-level full factorial design with relative saturation pressures between 0.0025 and 0.0425. This data set was used as the test set for the prediction of independent test data and will be further referred to as the test data set. A total of 24 measurements were identified as outliers according to ref 17, whereby 20 measurements of the calibration set and 4 measurements of the test set were removed. These measurements showed outlying high signals and were recorded in series. The compositions of the mixtures of both data sets are shown in Figure 2. It is also noticeable that the compositions of the test and calibration data are all different.

During all measurements, the polycarbonate was exposed to the analyte mixtures for 120 s and after that to synthetic air for 300 s. During exposure to analyte the data were recorded every 5 s, and during exposure to synthetic air with a time resolution of 10 s. Thus, the signals were recorded during 53 time slots, which will be further referred to as time channels. All measurements were done in random order. All data were autoscaled by subtracting the mean and dividing by the standard deviation for each variable.

Neural Networks. The neural networks implemented for this study belong to the class of the multilayer feed-forward back-propagation networks. Due to the numerous excellent textbooks describing these networks in detail,[18–21] only a short outline of the implementation for this study will be given.

(14) Johansen, K.; Arwin, H.; Lundström, I.; Liedberg, B. *Rev. Sci. Instrum.* **2000**, *71/9*, 3530–3538.

(15) Jung, L. S.; Campbell, C. T.; Chinowsky, T. M.; Mar, M. N.; Yee, S. S. *Langmuir* **1998**, *14*, 5636–5648.

(16) Kretschmann, E.; Raether, H. *Z. Naturforsch.* **1968**, *23A*, 2135–2136.

(17) Tetko, I. V.; Villa, A. E. P. *Neural Networks* **1997**, *10*, 1361–1374.

For both analytes, separate networks were used. The topology consisted of one output unit, four hidden units, and as many input units as time channels used. The nets were fully connected. The training included a maximum of 1000 learn cycles. An advanced variant of back-propagation was used as the learning scheme, called resilient propagation (Rprop),[22] with a δ starting value of 0.1, a δ upper value of 2, and a weight decay of 3. A hyperbolic tangent was used as the activation function for the hidden layer, and a linear activation function was used for the output layer. All calculations were performed by a new implementation of the Stuttgart Neural Network Simulator,[23,24] on a personal computer.

BP networks are often affected by an effect called overtraining.[25] An overtrained ANN memorizes the small calibration data set instead of generalizing the data and consequently performs badly on new data, e.g., on test data sets. In this work, the overtraining was anticipated by the so-called early stopping.[26] Early stopping was implemented by stopping the training when the error of cross-validation of the calibration data starts going up, as the net may start losing its generalization ability at this moment. Further, to prevent overtraining, the number of training objects should be several times more than the number of adjustable parameters of the ANN.[27] As every link and every hidden neuron contains one adjustable parameter, the feature selection performed in the last section of this study also helped to efficiently prevent overtraining.

Feature Selection. A greedy algorithm presented by Vinod and Ghose[28] was used for the feature selection. The network growing algorithm starts with an empty network and tries to minimize the sum square error of prediction by successively inserting neurons with two input and one output links, whereby the output link is connected to an output neuron. A modified version of the algorithm was used in this work, which is optimized for the feature selection of sensors:

(i) Instead of estimating the reduction of the error by utilizing the gradient of the error surface by varying the weights of the inserted element, the modified algorithm calculates the reduction of the error by retraining the network after the insertion of the new element and thus utilizes the gradient of the total error surface. This modification improves the selection of variables showing similar variances with the disadvantage of an increased computation time.

(ii) Not only units with two input links and one output link but also units with one input link and one output link and even single links can be inserted, allowing any kind of topology being built.

(iii) The stopping criterion of an absolute error limit was replaced by the stopping criterion of a minimal error decrease of 5% for the insertion of a new element.

(iv) A maximum number of 10 input neurons is allowed.

A total of 200 single output networks were built for the prediction of the concentrations of each analyte using this greedy algorithm.

Comparison of the Results. The performance of the different neural networks was measured by comparing the root-mean-square error of the prediction:

$$\mathrm{RMSE} = \sqrt{\frac{\sum_{i=1}^{N}(\hat{y}_i - y_i)^2}{N}} \qquad (2)$$

where N is the total number of data, $\hat{y}_i$ is the predicted concentration, and y_i is the true concentration. The relative root-mean-square error is calculated as

$$\mathrm{RMSE}_{\mathrm{rel}} = \left\{\sqrt{\frac{\sum_{i=1}^{N}(\hat{y}_i - y_i)^2}{N}}\right\} \Big/ \left\{\frac{\sum_{i=1}^{N} y_i}{N}\right\} \qquad (3)$$

As the initial weights of an ANN are randomly assigned, the solution found by a neural network for the calibration data is sensitive to the initial conditions stopping in another local minimum for each run. To find a robust ANN, which is not influenced by accidental training runs giving by chance an overestimated prediction of the test data, an approach similar to recent literature[29−30] was followed in this study: 21 ANN were trained with different initial weights but the same topology. For comparing different topologies, e.g., during the feature selection process, the different topologies were compared by the median of the RMSE of the cross-validated calibration data of the 21 runs. For the prediction of the test data, the network with the smallest RMSE of the cross-validated calibration data was used in contrast to many studies using the best prediction of the test data out of many runs.

RESULTS AND DISCUSSION

Pure Analytes. In Figure 3a, the shift of the surface plasmon resonance wavelength is shown during exposure of the device to an alternating sequence of synthetic air and different concentrations of methanol up to a relative saturation pressure (p_i/p_{i0}) of 0.062. During exposure to analyte, the resonance wavelength increases, which means that the refractive index increases. At first glance, this is astonishing since methanol ($n_D = 1.329$) has a lower refractive index than the polycarbonate layer ($n_D = 1.58$). Due to the lower refractive index of methanol, its sorption into the

(18) Zupan, J.; Gasteiger, J. *Neural networks in chemistry and drug design* 2nd ed.; Wiley-VCH: Weinheim, Germany, 1999.
(19) Patterson, D. *Artificial neural networks, theory and applications*; Prentice Hall Inc.: Upper Saddle River, NJ, 1996.
(20) Principe, J.; Euliano, N.; Lefebvre, W. *Neural and adaptive systems: Fundamentals through simulations*; John Wiley & Sons Inc.: New York, 2000.
(21) Kaykin, S. *Neural networks a comprehensive foundation*; Prentice Hall Inc.: Upper Saddle River, NJ, 1999.
(22) Riedmiller M.; Braun H. *Rprop−a fast adaptive learning algorithm. Technical report*; University of Karlsruhe, Germany, 1992.
(23) Zell, A. *SNNS Stuttgart Neural Network Simulator*: http://www-ra.informatik.uni-tuebingen.de/SNNS/, 2002.
(24) Rapp, F. R. Kalibrierung und Validierung von Sensorarrays unter Einsatz Neuronaler Netze und genetischer Algorithmen. Master Thesis, University of Tübingen, Germany, 1996.
(25) Weigend, A. *Proceedings of the 1993 Connectionist Models Summer School*; 1994; pp 335−342.
(26) Sarle, W. S. *Proceedings of the 27th Symposium on the Interface of Computing Science and Statistics*; 1995; pp 352−360.
(27) Kolen, J. F.; Pollack, J. B. In *Advances in Neural Information Processing System*; Lipmann, R. P., Moody, J. E., Touretsky, D. S., Eds.; Morgan Kauffman Publishers: San Mateo, CA, 1993; pp 860−867.
(28) Vinod, V. V.; Ghose, S. *Neurocomputing* **1996**, *10*, 55−69.
(29) Despagne, F.; Massart D. L.; Chabot P. *Anal. Chem.* **2000**, *72*, 1657−1665.
(30) Dieterle, F.; Nopper, D.; Gauglitz, G. *Fresenius J. Anal. Chem.* **2001**, *370*, 723−730.

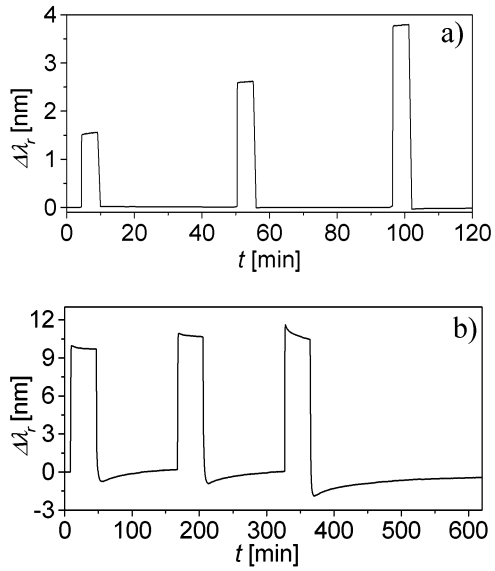

Figure 3. (a) Time-resolved measurement of methanol up to a relative saturation pressure of 0.062. (b) Time-resolved measurement of methanol at relative saturation pressures of 0.31, 0.62, and 0.80.

polycarbonate by displacing the polycarbonate within the evanescent field would cause a negative change of the refractive index. Instead, an increase of the refractive index is observed. This increase can be explained by the occupation of micropores of the polycarbonate by the analyte: Makrolon is a microporous glassy polymer with a mean size of the pores of 0.1 nm^3,[31] whereas the volumes of methanol (0.068 nm^3) and ethanol (0.097 nm^3) are slightly smaller than the mean size of the pores of Makrolon. Without the analyte being present in the gaseous phase, the micropores are filled with air, which has a lower refractive index than the analyte. While the analyte is sorbing into the micropores and thereby replacing the air, the change of the refractive index and therefore the change of the resonance wavelength are positive. As can be seen in Figure 3a, the sorption at these concentrations is fast and reversible. The layer is highly stable and the mean drift is 5.3×10^{-4} nm/h, which corresponds to only 0.01% of the maximum response.

In Figure 3b, the shift of the surface plasmon resonance wavelength is shown while the device was exposed to an alternating sequence of synthetic air and relative saturation pressures of methanol of 0.31, 0.62, and 0.80. At these high concentration levels, the refractive index increases rapidly at the beginning of the analyte exposure. However, during a longer exposure of the polycarbonate to methanol, the refractive index further decreases. This effect reinforces with higher methanol concentrations and can be explained by a further swelling of the polycarbonate layer after the occupation of the micropores. The fast decrease of the refractive index during the exposure to synthetic air means that the analyte quickly disappears out off the micropores. The refractive index even decreases below the original value before the exposure to methanol vapor. The original value is gradually reached while the swelling of the polycarbonate diminishes. Thus, even at these high concentration levels, the swelling of the polymer is reversible.

(31) Dlubek, G.; Clarke, A.; Fretwell, H.; Dugdale, S. B.; Alam, M. A. *Phys. Status Solidi A* **1996**, *157*, 351−364.

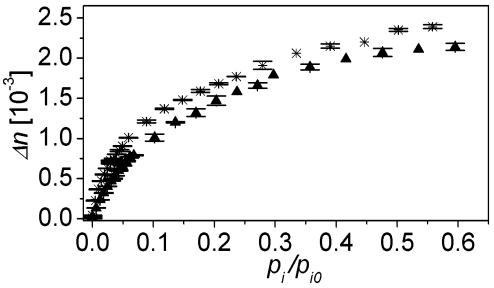

Figure 4. Calibration curves of methanol and ethanol. Signals are recorded after 30-min analyte exposure. Calibration points of methanol are represented by triangles, and calibration points of ethanol are represented by stars.

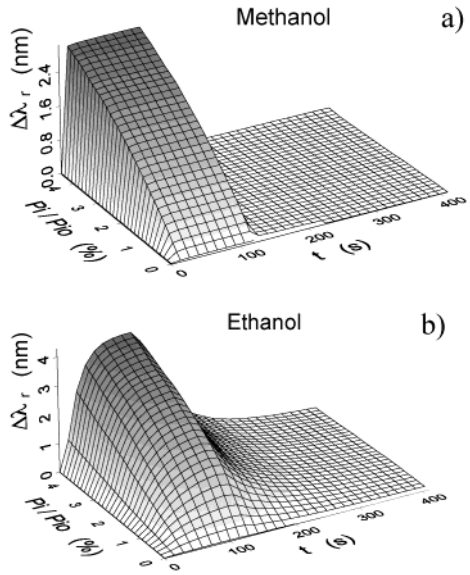

Figure 5. Signal shifts versus exposure time and concentration of (a) methanol and (b) ethanol.

The calibration curves of methanol and ethanol are shown in Figure 4. The difference in the refractive index is recorded between the exposure to synthetic air and after 30-min exposure to analyte. The standard deviation of three measurements is given by the error bars. At higher concentrations, a smaller increase of the refractive index with an increasing methanol or ethanol concentration can be observed. The curvature of the calibration curve can be explained by the limited number of micropores. The change in the refractive index during exposure to ethanol is only slightly higher than during exposure to methanol since the refractive index of ethanol is slightly higher than the refractive index of methanol. The calibration curves being nonlinear, both analytes can be detected with the highest sensitivity at small concentrations.

The changes of the resonance wavelength of methanol and ethanol depending on concentration and time are plotted in Figure 5a and b, respectively, up to a relative saturation pressure of 0.045. The polycarbonate layer was exposed to different concentrations of methanol or ethanol vapors for 120 s. Then it was exposed to synthetic air for 300 s. The fast response time of methanol can be confirmed. Ten seconds of exposure to methanol vapor is enough to reach equilibrium between the methanol vapor and the methanol, which is sorbed into the polycarbonate layer, and thus the resonance wavelength does not change further. In contrast,

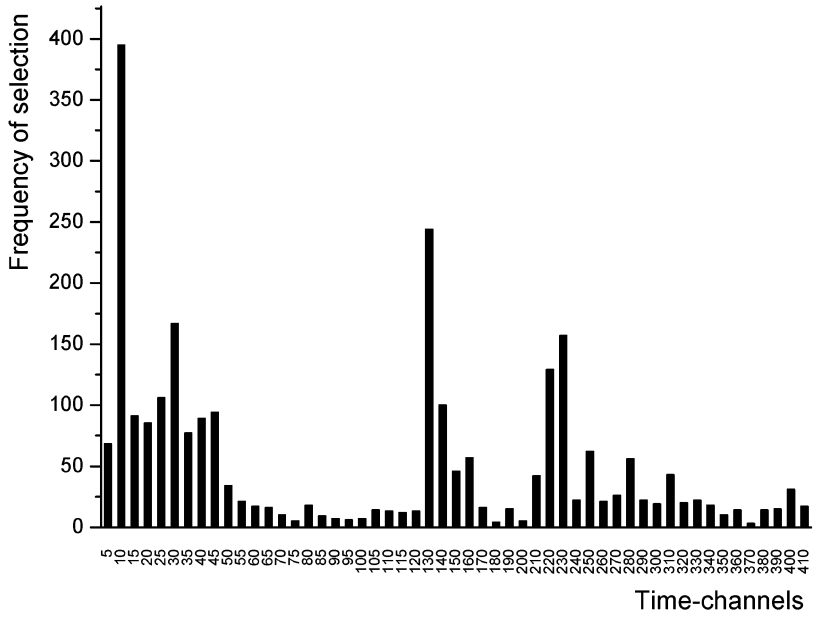

Figure 6. Frequency of the selection of the various time channels during the feature selection process.

even after 120 s of exposure of the polycarbonate layer to ethanol vapor, equilibrium was not reached. However, after 120 s, the signals of ethanol are larger than the signals of methanol for the same relative saturation pressure. Since the diffusion of ethanol is a lot slower, the signals at short exposure times are lower compared to methanol.

In summary, it may be said that at small concentrations the signal responses of the sensor are fast and reversible, and the dynamic responses to both analytes differ in shape when recorded over time. Therefore, a discrimination of methanol and ethanol in mixtures should be possible by measuring the signals of this single sensor setup during different times and thus by creating a virtual time channel array instead of using a real array of sensors coated with different polymers.

Mixtures. The multivariate calibration is based on the training of neural networks by the calibration data set and a subsequent prediction of the test data set. First, neural networks using all 53 time channels were investigated. The root-mean-square errors of the cross-validation and of the prediction of the independent test data set are listed in the first and fifth row of Table 1. The concentrations of the test samples were predicted with a relative RMSE of 3.32% for methanol and 4.11% for ethanol. The error of the independent test data is comparable to the error of the cross-validated calibration data for both analytes together, giving evidence that the models are highly predictive.

Although it is very tempting to use these very predictive neural nets including all available time channels, the high correlation of the time channels includes too much redundant information and thus inhibits the convergence of the model due to a very complex error surface. Use of only the set of time channels that produces the most predictive model not only improves the predictive ability of the model but also simplifies the model for the sake of easier interpretability.[32−35] For the selection of the most important variables (commonly called feature selection), the greedy algorithm described before was applied to the calibration data set. As inclusion of variables depends on the randomly generated initial parameters of the neural net, the selection results of different runs can be significantly different. Thus, the greedy algorithm was repeated 400 times in total. The plot of the frequencies of occurrence of the different time channels (Figure 6) shows that the variables in three time intervals are prominent: the beginning of exposure to analyte (10−45 s), when exposure to analyte has ended and exposure to synthetic air starts again (130−140 s), and additionally 100 s after the start of exposure to synthetic air (220−230 s). The first two intervals are the easiest to interpret as in accordance with Figure 4a and b the responses to both analytes differ most during these time intervals. The time interval around 220 s can be considered as a reference signal with practically no analyte remaining.

Table 1. Comparison of the RMSE of the Calibration and Test Data Using Different Networks and Time Channels

time channels	RMSE cross-validation ($\times 10^{-4}$)	RMSE test data ($\times 10^{-4}$)	rel test data (%)
	Methanol		
53	10.6	7.37	3.32
4	4.27	4.68	2.11
3	4.46	4.39	1.97
2	5.06	4.93	2.22
	Ethanol		
53	7.09	9.27	4.11
4	4.74	5.87	2.60
3	4.30	5.35	2.37
2	5.32	6.10	2.70

(32) Handels, H.; Roσσ, T.; Kreusch, J.; Wolff, H. H.; Pöppl, S. J. *Artif. Intell. Med.* **1999**, *16*, 283−297.
(33) Xu, L.; Zhang, W.-J. *Anal. Chim. Acta* **2001**, 477−483.
(34) Broadhurst, D.; Goodacre, R.; Jones, A.; Rowland, J. J.; Kell, D. B. *Anal. Chim. Acta* **1997**, 71−86.
(35) Herrero, A.; Ortiz, M. C. *Anal. Chim. Acta* **1999**, 245−259.

The final model is obtained by a stepwise approach in which the variables are entered according to the frequency of selections, and thus, as many models are build as variables are available. Each model is evaluated by the RMSE of the cross-validation of the calibration data. The smallest error of cross-validation was obtained by the model using only three time channels. According to Table 1, row 3 and row 7, the error of cross-validation is significantly lower using the time channels 10, 30, and 130 s than the model using all time channels. It is also lower than a model using four time channels (10, 30, 130, and 230 s). Thus, the third time interval seems to contain no significant additional information. The prediction of the test data by neural nets using three time channels (topology 3-4-1) shows an excellent low relative root-mean-square error of 1.97% for methanol and 2.37% for ethanol. The standard deviation of the signal from an individual vapor (referred to the mean of the signal) was calculated for the calibration curves of Figure 4 to 0.62% (methanol) and 0.98% (ethanol). These errors are caused by the noise of the spectrometer, inaccuracies of the gas mixing apparatus, and fluctuations of the measuring temperature and thus exist also for the measurement of mixtures. Therefore, the rather small increase of the errors shows the possibilities of the time-resolved measurements in combination with the evaluation with neural networks for a multicomponent analysis. An extension to the parallel quantification of more analytes should be possible for analytes showing different diffusion kinetics. The prediction of data is often demonstrated in so-called true predicted plots. In Figure 7, the true predicted plots of the test data and the cross-validation of the calibration data are shown. As the single predictions cannot be graphically resolved, the predictions of each concentration level are combined by the mean and standard deviation. The predictions of all concentrations are marked by a very small standard deviation and by the absence of systematic errors.

The small number of variables allows an efficient sensitivity analysis.[36] The values of two time channels were systematically varied between the measured minimum and maximum signal shifts of the time channels and the third time channel was kept constant in the middle of the measured signal shift. The neural nets of the preceding paragraph were fed with these three time channels. The concentrations calculated by the neural nets are plotted versus the two varying time channels in Figure 8. The top row of this figure shows the prediction of the concentration of methanol and ethanol, depending on the signal of the time channels 10 (*x*-axis) and 30 s (*y*-axis). The prediction of methanol is determined by the ensemble of both time channels. This is in accordance with Figure 4, which demonstrates that the sorption process of methanol has come to a steady state after 10 s. Hence, a high signal after 10 s caused by a high concentration of methanol automatically induces a high signal after 30 s. The top right plot of Figure 8 shows that the prediction of ethanol is practically not influenced by the time channel 10 s explainable by the variance of this time channel being mainly caused by the sorption of methanol (Figure 5a). Nevertheless, the prediction of ethanol is nearly linearly correlated with the signal of the time channel 30 s. The bottom row of Figure 8 shows the prediction of the concentration depending on the signal of the time channels 10 (*x*-axis) and 130 s (*y*-axis). The plane parallel to the *y*-axis

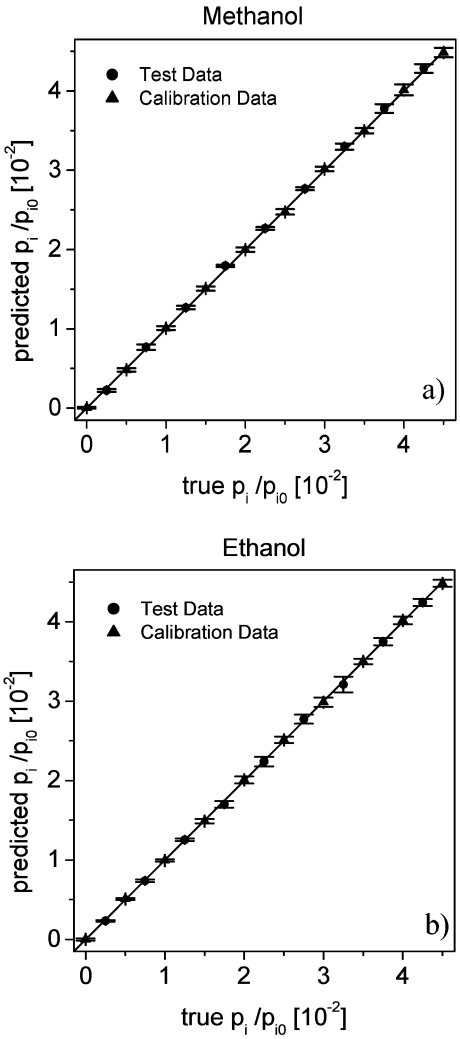

Figure 7. Predicted concentrations (expressed as relative saturation pressures) of (a) methanol and (b) ethanol versus the true concentrations for the test and calibration data.

demonstrates that the prediction of methanol is practically independent from the time channel 130 s. However, the prediction of ethanol highly depends on the signal of time channel 130 s. The plots of Figure 8 top right and bottom right are nearly identical except for the higher dynamics of time channel 130 s.

In summary, it may be said that the prediction of methanol depends on the combination of the time channels 10 and 30 s whereas the prediction of ethanol depends on the time channel 30 s and on the time channel 130 s. The similar dependencies of the predictions of ethanol on the time channels 30 and 130 s indicate that the time channel 130 s could be rendered unnecessary by calculating the concentrations of methanol using the signal of time channel 10 s and by calculation of the concentration of ethanol by the ratio of the signals after 10 and 30 s. Thus, neural networks of the topology 2-4-1 were trained using only the time channels 10 and 30 s. Table 1 demonstrates that these small networks perform well, predicting both analytes with relative errors of only 2.22% and 2.70%. The only small deterioration of the predictive ability is overcompensated by the fact that measurement time can be reduced from 130 to 30 s. In addition, shortening of the time for the polymer being exposed to the analyte results in the sorption of less ethanol into the polymers. Therefore, the

(36) So, S.-S.; Karplus, M. *J. Med. Chem.* **1996**, *39*, 1521−1530.

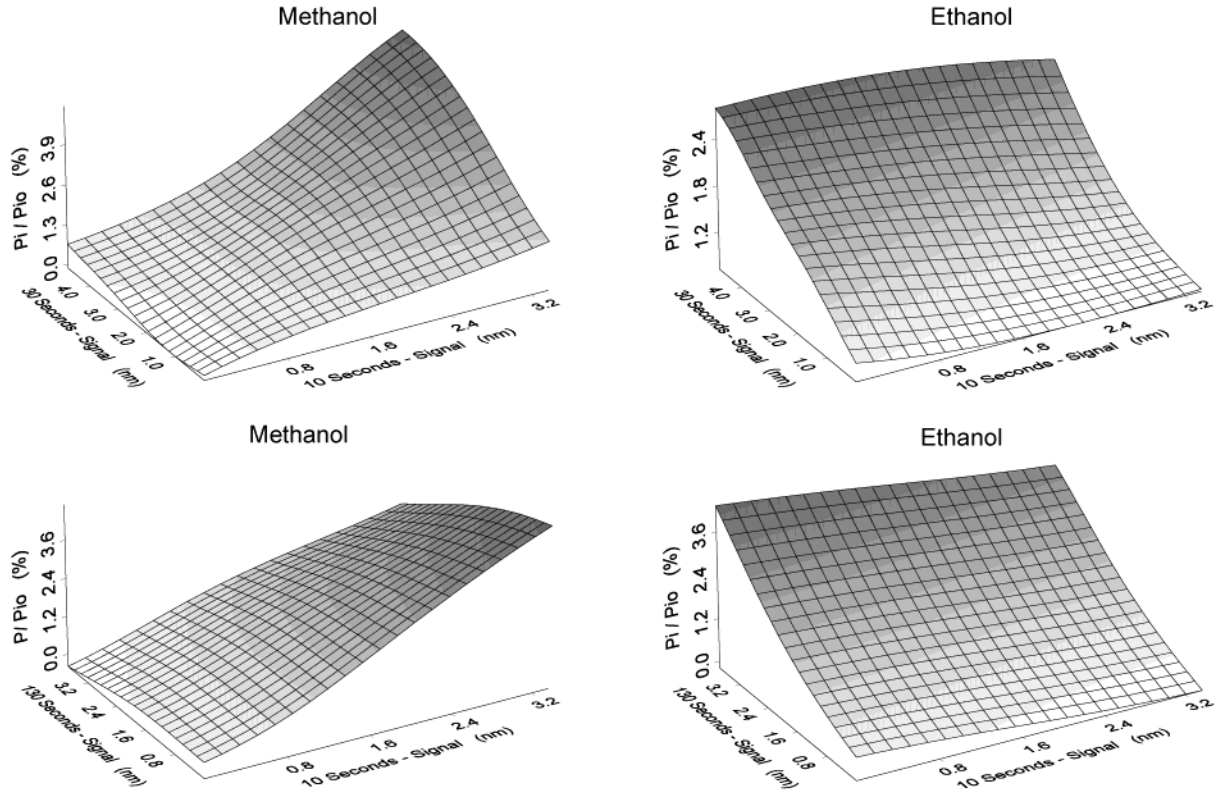

Figure 8. Calculated concentrations of the sensitivity analysis versus the two time channels varied.

desorption of ethanol needs less time to be completed. Consequently, the time between different measurements can be considerably shortened.

CONCLUSION

It has been shown that the polycarbonate Makrolon provides a sensitive, stable, and reversible sensor layer, which is highly selective due to the sorption of the analytes into the micropores of the polymer. The combination of the polycarbonate as sensitive layer, the time-resolved measurements, the data analysis by neural networks, and a feature selection process allowed a quantitative multicomponent analysis of ethanol and methanol. Both analytes have been successfully quantified in mixtures with impressive low errors of 2.0% and 2.4%, respectively. It was demonstrated that the measurement time could be reduced to 30 s with nearly no deterioration of the predictive ability.

More investigations will be performed on a further shortening of the measurement time by a reduction of the layer thickness by varying the concentrations of the polymer solutions during the preparation. An extension to the quantification of ternary mixtures should be possible. Additionally, other small analytes, the presence of a varying ambient humidity,[37] and other microporous polymers will be investigated, since the principle of diffusion constants depending on size is adaptable to a broad variety of analytes.

ACKNOWLEDGMENT

This work was supported by the AiF (OSYRIS), the Deutsche Forschungsgemeinschaft (Graduiertenkolleg "Analytische Chemie"), and by the Fonds der Chemischen Industrie. Fred-Reiner Rapp ia acknowledged for the software NEMO, which is a new implementation of the SNNS kernel.

Received for review June 3, 2002. Accepted July 24, 2002.

AC0258204

(37) Dickert, F. L.; Hayden, O.; Zenkel, M. E. *Anal. Chem.* **1999**, *71*, 1338−1341.